Int. J. Electrochem. Sci., 9 **(2014)** 3904 - 3916

International Journal of
ELECTROCHEMICAL
SCIENCE
www.electrochemsci.org

Synthesis, Stability and DC-electrical Conductivity of Vanadium and Chromium Dual Doped $LiMn_2O_4$ Spinals as Cathode Material for Use in Lithium Rechargeable Batteries

Fawaz A. Saad[1], *Morsi M. Abou-Sekkina*[2], *Abdalla M\. Khedr*[1,2,*], *Fouad G. El-Metwaly*[2,3,*]

[1] Chemistry Department, College of Applied Sciences, Umm Al-Qura University, Makkah, Saudi Arabia
[2] Chemistry Department, Faculty of Science, Tanta University, Tanta, Egypt
[3] Chemistry Department, Faculty of Science, Jazan University, Jazan, Saudi Arabia
[*]E-mails: abkhedr2010@yahoo.com (A.M. Khedr), fouadmandoor@yahoo.com (F.G. El-Metwaly).

Received: 3 March 2014 / *Accepted:* 5 April 2014 / *Published:* 14 April 2014

V^{5+} and Cr^{6+} double doped nano lithium manganese oxide spinels $Li[V_xCr_xMn_{2-2X}]O_4$, (x=0.00, 0.02, 0.05 %)] were synthesized by doping the pure spinel $LiMn_2O_4$ with vanadium and chromium ions as cathode materials for rechargeable batteries applications. These cathode materials were characterized by thermal gravimetric and differential thermal analysis (TG/DTA), x-ray powder diffractometry (XRD), scanning electron microscopy (SEM) and infrared spectroscopy (IR) measurements. XRD and SEM studies confirmed the nano materials size for all prepared spinels. $LiMn_2O_4$ and $Li[V_{0.05}Cr_{0.05}Mn_{1.9}]O_4$ spinels were irradiated by γ-irradiation (10 and 30 kGy). Direct-current (DC) electrical conductivity measurements indicated that these samples are semiconducting and their conductivity was strongly affected by the dopant cations and γ-irradiation.

Keywords: lithium ion battery, vanadium and chromium co-doped spinels, γ--ray effect

1. INTRODUCTION

Rechargeable Li-batteries offer the highest energy density of any battery technology, and they power most of today's portable electronics [1]. Also, Li-ion batteries are playing a leading role in the automobile markets which is presently aimed to develop low emission cars, such as hybrid electric vehicles and plug-in hybrid electric vehicles and zero emission, full electric vehicles. To make these systems suitable for electric vehicle sector, further improvements in energy and power density are required [2]. Portable electronic devices are now essential components of our daily lives, and whether the device in question is a toy, a mobile phone, or a laptop computer, for a power source it relies on

batteries [3]. To meet the demands of portable devices and electric vehicles, it is vital to develop the cathode materials for Li-ion battery. Among the cathode materials, $LiMn_2O_4$ has many advantages, such as low toxicity, cost efficiency, environmental friendliness, and relatively high energy density compared to other transition metal oxides, such as lithium cobalt oxide or lithium nickel oxide [4–6]. However, the disadvantage is that spinel $LiMn_2O_4$ suffers from severe capacity fading, especially at higher temperature (55 °C) during discharging/charging. This limits its cycle ability and does not allow its commercialization [7]. To prevent it, $LiMn_2O_4$ has been doped by partial substitution of Mn^{3+} by several iso- or aliovalent cations such as Li, Cu, Ni, Co, Al, Cr, Tb and Sm [8-12]. There are various factors that account for the capacity fading such as Jahn–Teller distortion, lattice instability [13], slow dissolution of manganese into the electrolyte [14], a two- phase unstable reaction [15], and particle-size distribution [16]. Single-ion-doped $LiMn_2O_4$ spinels could not account for all the factors responsible for the severe capacity loss during cycling. Multiple cations substituted $LiMn_2O_4$ has been reported and it has been pointed out that co-doping has a synergistic effect on the improvement of the cycling life [17-19]. Therefore, the combined synergistic effect of vanadium and chromium in the Mn-spinel is expected to enhance the electrochemical performance by stabilizing the spinel $LiMn_2O_4$. In this study, the stabilizing effects of the multivalent cations V^{5+} and Cr^{6+} in the spinel $LiMn_2O_4$ have been investigated. The aim of this investigation is to determine the effect of low content V/Cr co-doping on the spinel $LiMn_2O_4$ and also to determine the optimized dopant levels to achieve maximum capacity and greatest stability.

2. EXPERIMENTAL

All the chemicals were used directly without any further purification before use.

2.1. Synthesis of pristine and V–Cr-doped $LiMn_2O_4$

$LiMn_2O_4$ and $Li[V_xCr_xMn_{2-2X}]O_4$, (x= 0.02, 0.05 %)] compounds were synthesized by solid state reaction method [20, 21]. Stoichiometric amounts of the reactants, $LiOH.H_2O$ (99%) and manganese carbonate (99.5%) were carefully mixed and appropriate amounts of NH_4VO_3 and $(NH_4)_2CrO_7$ were added. The mixtures were ball milled to assure uniform distribution of the small amounts of dopants. Then, the mixtures were pre-sintered at 60^{o}C for 4 h. Finally, the samples were reground and pressed into pellets and sintered in air at 850^{o}C for 8 h, with a heating rate of 10^{o}C/min.

2.2. Materials characterization

X-ray diffraction (XRD) for the materials were measured by the instrument Phillips (Holland) x-ray diffractometer (PW 1729 x-ray generator, PW 1840 diffractometer control, PM 8203A, one line recorder) with Cu Kα radiation (λ = 1.54056 Å) in 2θ = 10 ∼ 80°. The morphology of the prepared materials were investigated by scanning electron microscope (SEM, JSM- 5300LV, Japan). The

thermal gravimetric analysis (TGA) was carried out in a dynamic nitrogen atmosphere (20 ml min^{-1}) with a heating rate of 10°C min^{-1} using a Shimadzu TG-50 thermogravimetric analyzer. DTA of green samples (uncalcined) were recorded by a Du Pont instruments 990 thermal analyzer (England) with a heating rate of 10°C min^{-1} at Central Laboratory, Tanta University. IR spectra were measured using a Perkin–Elmer 1430 IR spectrophotometer within the range 1000-200 cm^{-1} for all samples as KBr discs. DC-electrical conductivity of all samples sintered at 850°C for 8 hr was measured using the two terminal DC-electrical conductivity method, where the pellets of the samples were coated with silver paste, inserted between the two copper probe of the circuit using a Akeithly 175 multimeter (USA). This was done at the temperature range from room temperature up to 370°C. The temperature was measured by a calibrated chromel-alumel thermocouple placed firmly at the sample during measurements.

2.3. Study the γ-ray effect on the synthesized samples

$LiMn_2O_4$ and $Li[V_{0.05}Cr_{0.05}Mn_{1.9}]O_4$ spinels were exposed to **γ**-irradiation with different doses (10 KGy and 30 KGy) at National Center for Radiation Research and Technology, Nasr City, Cairo, Egypt. An Indian ^{60}Co gamma cell (2000.Ci) was used as a gamma ray source with a dose rate of 1.5 Gy/sec (150 rad/sec) [22]. Gy (a gray) is the SI derived unit of absorbed dose and specific energy (energy per unit mass). Such energies are usually associated with ionizing radiation of gamma particles. It is defined as the absorption of one joule of energy in the form of ionizing radiation by one kilogram of tissue. In the SI basic units, a gray is expressed as $m^2 \cdot s^{-2}$ [23].

3. RESULTS AND DISCUSSION

3.1. Thermal analysis (TGA and DTA)

The thermal analysis of the inorganic compounds gives very good information on their structures, properties, nature of intermediate and final products of their thermal decomposition [24]. From the TGA curves, the mass loss can be calculated for the different decomposition steps and compared with those for the suggested formula [25]. The thermogravimetric (TGA and DTA) curves of the green sample that was fired to give the $LiMn_2O_4$ nano spinels by solid state method are presented in figures 1 and 2. The weight loss at 70-120°C is caused by the volatilization of adsorbed water and other organic substances, which corresponding to weak endothermic peaks in DTA curve. The weight loss of 5% due to loss of H as a result of decomposition LiOH to Li_2O within 164–291°C temperature range appeared as a weak exothermic peak at 169°C in the DTA curve. Finally, the weight loss of 18% in the temperature range of 291–690°C corresponds to combustion of residual organic moiety and loss of excess oxygen from the precursor (revealed as a broad exothermic peak at 500°C in the DTA curve). In the temperature range of 690°C to 900°C, there is nearly constant weight; only phase transfer occurs in this range, continuing until the stable spinel phase.

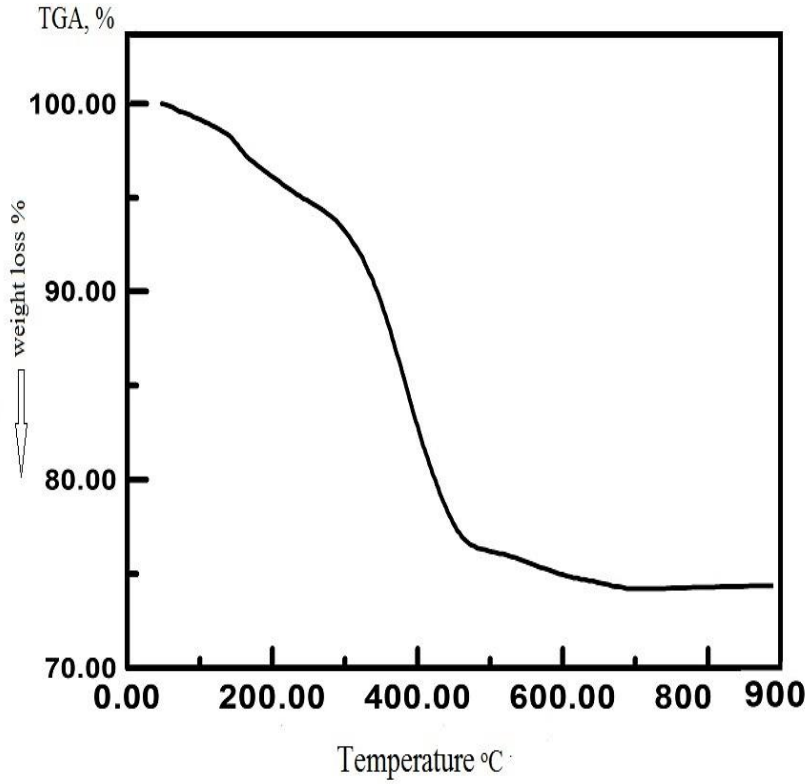

Figure 1. TGA curve of the green sample that gives $LiMn_2O_4$ spinel by solid-state method.

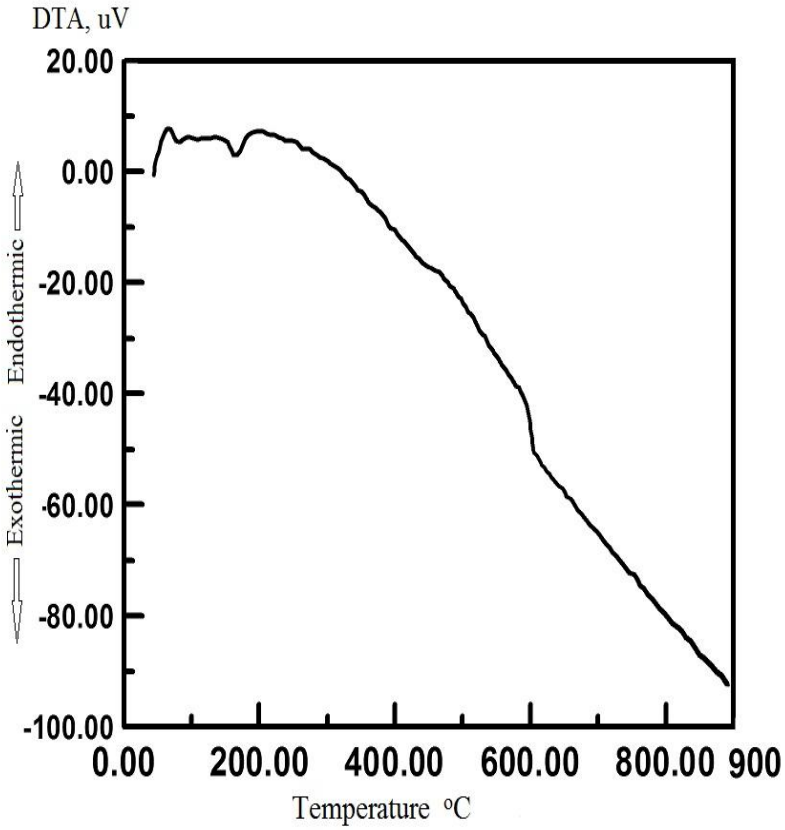

Figure 2. DTA curve of the green sample that gives $LiMn_2O_4$ spinel by solid state method.

3.2. X – ray diffraction analysis

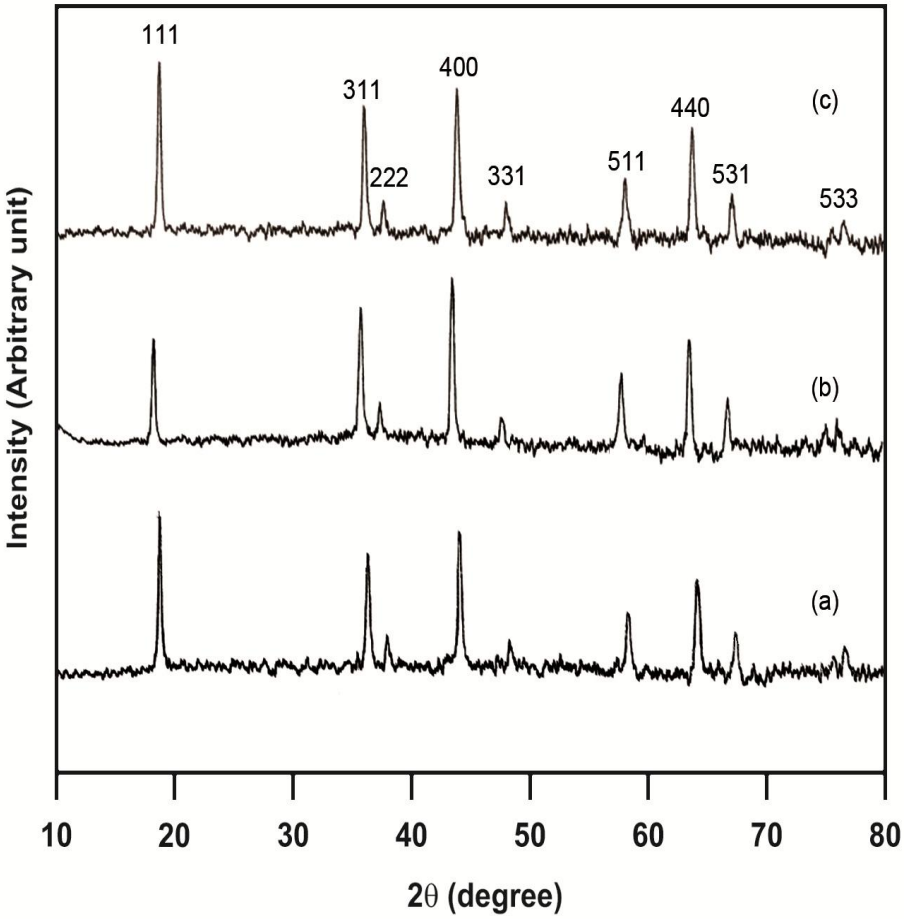

Figure 3. X-ray diffraction patterns of pure and doped nano $Li[V_xCr_xMn_{2-2X}]O_4$ spinels: (**a**) pure $LiMn_2O_4$, (**b**) $Li[V_{0.02}Cr_{0.02}Mn_{1.96}]O_4$, and (**c**) $Li[V_{0.05}Cr_{0.05}Mn_{1.90}]O_4$.

XRD patterns for pristine $LiMn_2O_4$, $Li[V_{0.02}Cr_{0.02}Mn_{1.96}]O_4$, and $Li[V_{0.05}Cr_{0.05}Mn_{1.90}]O_4$ are depicted in figure 3. As expected, such small amounts of substituting metal ions do not affect the spinel structure; even for the higher dopant concentrations, a well-defined cubic spinel structure is retained. The spinel structure with space group Fd3m in which the lithium ions occupy the tetrahedral (8a) sites and the Mn^{3+}/Mn^{4+} ions, as well as the doped metal ions reside at the octahedral (16d) sites, can be identified according to the indexed major peaks [26]. All the patterns can be assigned to well-crystallized spinel $LiMn_2O_4$ (JCPDS No. 35-0782) with no impurity peaks at different dopants concentrations. All the peak reflections perfectly match with the Joint Committee of Powder Diffraction Standard (JCPDS card No. 35-782). Spectral profiles of undoped and V and Cr-doped spinels exhibit a high degree of crystallinity and better phase purity. It is evident that all the peaks corresponding to (111), (311), (222), (400), (331), (551), (440), (531), and (533) hold striking similarity to those reported in previous communications [27, 28].

Table 1. Lattice constant and unit cell parameters of $LiMn_2O_4$ and $Li[V_xCr_xMn_{2-2X}]O_4$ compounds before and after γ-irradiation

No	Sample	Lattice Constant, a (Å)	Unit cell Volume ($Å^3$)
1	$LiMn_2O_4$	8.186	547
2	$Li[V_{0.02}Cr_{0.02}Mn_{1.96}]O_4$	8.246	561
3	$Li[V_{0.05}Cr_{0.05}Mn_{1.90}]O_4$	8.337	579
4	$LiMn_2O_4$ γ-irradiated with 10 kGy	8.244	560
5	$LiMn_2O_4$ γ-irradiated with 30 kGy	8.327	577
6	$Li[V_{0.05}Cr_{0.05}Mn_{1.90}]O_4$ γ-irradiated with 10 kGy	8.350	582
7	$Li[V_{0.05}Cr_{0.05}Mn_{1.90}]O_4$ γ-irradiated with 30 kGy	8.360	584

Table 1 lists the lattice constant and unit cell parameters of $LiMn_2O_4$, $Li[V_{0.02}Cr_{0.02}Mn_{1.96}]O_4$, and $Li[V_{0.05}Cr_{0.05}Mn_{1.90}]O_4$ compounds before and after irradiation process, which are calculated from the XRD data using Scherrer's equation [29].

3.3. Gamma radiation effect

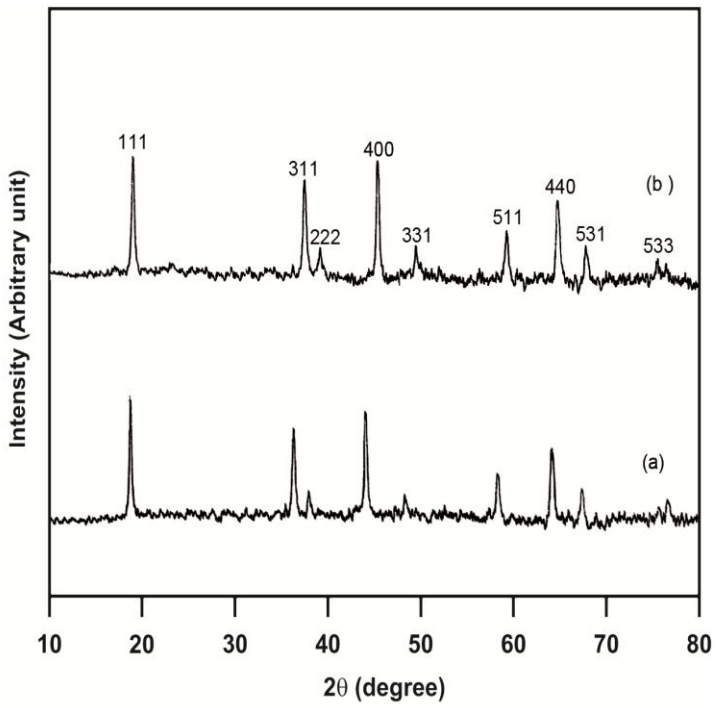

Figure 4. X-ray diffraction patterns of γ-irradiated pure $LiMn_2O_4$: (**a**) $LiMn_2O_4$ spinel γ-irradiated with 10 kG*y*, and (**b**) $LiMn_2O_4$ spinel γ-irradiated with 30 kG*y*.

Gamma radiation, refers to electromagnetic radiation of extremely high frequency and therefore high energy per photon. Gamma rays are ionizing radiation, and are thus biologically hazardous. They are classically produced by the decay from high energy states of atomic nuclei

(gamma decay). Ultrahigh energy gamma-ray (UHEGR) denotes gamma radiation with the shortest wavelengths (between 10^{-20} and 10^{-23} meter), with photon energies in the range from 10^{14} to 10^{17} electron-volts (eV) [30]. When a gamma ray passes through matter, the probability for absorption is proportional to the thickness of the layer, the density of the material, and the absorption cross section of the material.

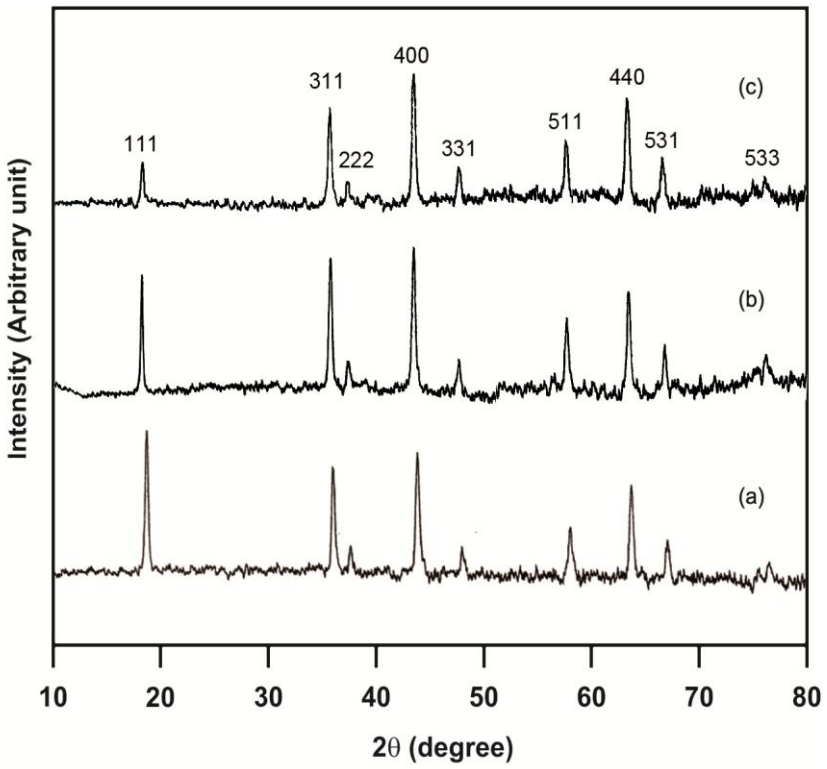

Figure 5. X-ray diffraction patterns of non irradiated and γ-irradiated $Li[V_{0.05}Cr_{0.05}Mn_{1.90}]O_4$: (**a**) Non irradiated $Li[V_{0.05}Cr_{0.05}Mn_{1.90}]O_4$ spinel, (**b**) $Li[V_{0.05}Cr_{0.05}Mn_{1.90}]O_4$ spinel γ-irradiated with 10 kG*y*, and (**c**) $Li[V_{0.05}Cr_{0.05}Mn_{1.90}]O_4$ spinel γ-irradiated with 30 kG*y*.

As it passes through matter, gamma radiation ionizes via three processes: the photoelectric effect, Compton scattering, and pair production. Pair production becomes possible with gamma energies exceeding 1.02 MeV, and becomes important as an absorption mechanism at energies over 5 MeV. By interaction with the electric field of a nucleus, the energy of the incident photon is converted into the mass of an electron-positron pair. Any gamma energy in excess of the equivalent rest mass of the two particles (totaling at least 1.02 MeV) appears as the kinetic energy of the pair and in the recoil of the emitting nucleus. At the end of the positron's range, it combines with a free electron, and the two annihilate, and the entire mass of these two is then converted into two gamma photons of at least 0.51 MeV energy each (or higher according to the kinetic energy of the annihilated particles) [31]. The secondary electrons (and/or positrons) produced in any of these three processes frequently have enough energy to produce much ionization themselves. Additionally, high energy gamma rays (more than 10 MeV) can interact with atomic nuclei resulting in ejection of particles in photodisintegration,

or in some cases, even nuclear fission (photofission) [31]. Figures 4 and 5 show x-ray diffraction patterns of pure $LiMn_2O_4$ and doped $Li[V_{0.05}Cr_{0.05}Mn_{1.90}]O_4$ γ-irradiated with 10 and 30 kG*y*. It can be seen from the patterns that all diffraction peaks are very strong, which indicating that the samples have good cubic crystal structure. The peaks are obviously shifted to lower angle upon high irradiation dose (30 kG*y*), in case of pure $LiMn_2O_4$ (figure 4). Slightly small shifts are observed in case of doped $Li[V_{0.05}Cr_{0.05}Mn_{1.90}]O_4$ upon high irradiation dose, which indicates high stability of the doped samples against ultrahigh energy gamma-ray [30]. These shifts are likely to be caused by the Jahn-Teller effect giving tetragonal distortion and leading to a splitting of the ground state [32]. On successive gamma irradiation, vanadium and chromium ions in $LiMn_2O_4$ host seem to suppress any possible alteration compared with undoped spinel.

3.4. Scanning electron microscopy (SEM)

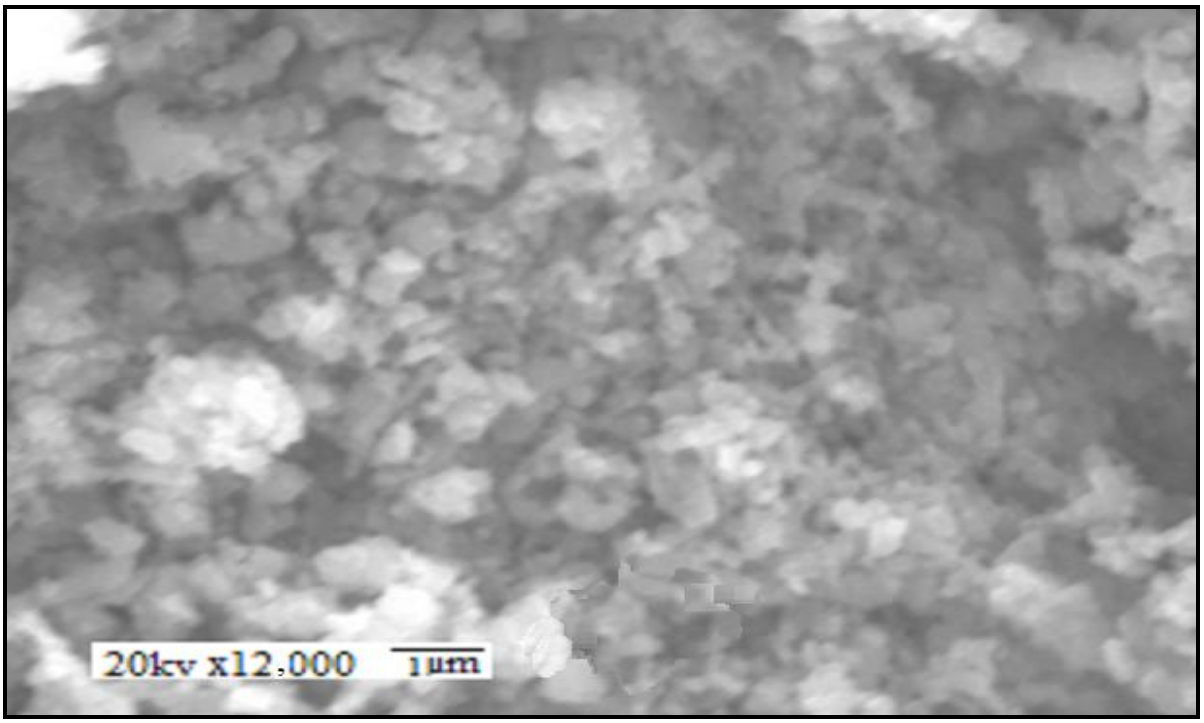

Figure 6. SEM image of $LiMn_2O_4$ nanospinel.

The morphology of pure and doped samples was investigated by scanning electron microscopy (SEM) after coating the samples with gold. The scanning electron micrographs of pure $LiMn_2O_4$ and co-doped $Li[V_{0.05}Cr_{0.05}Mn_{1.90}]O_4$ are presented in figures 6 and 7. As displayed in the micrographs, the composite has a narrow particle size distribution of about 1 μm, in agreement with lattice constant and unit cell parameter values calculated from the x-ray data (Table 1). The small uniform and narrow particle size distribution of the composite are favorable for electrochemical properties of high rate capability [33].

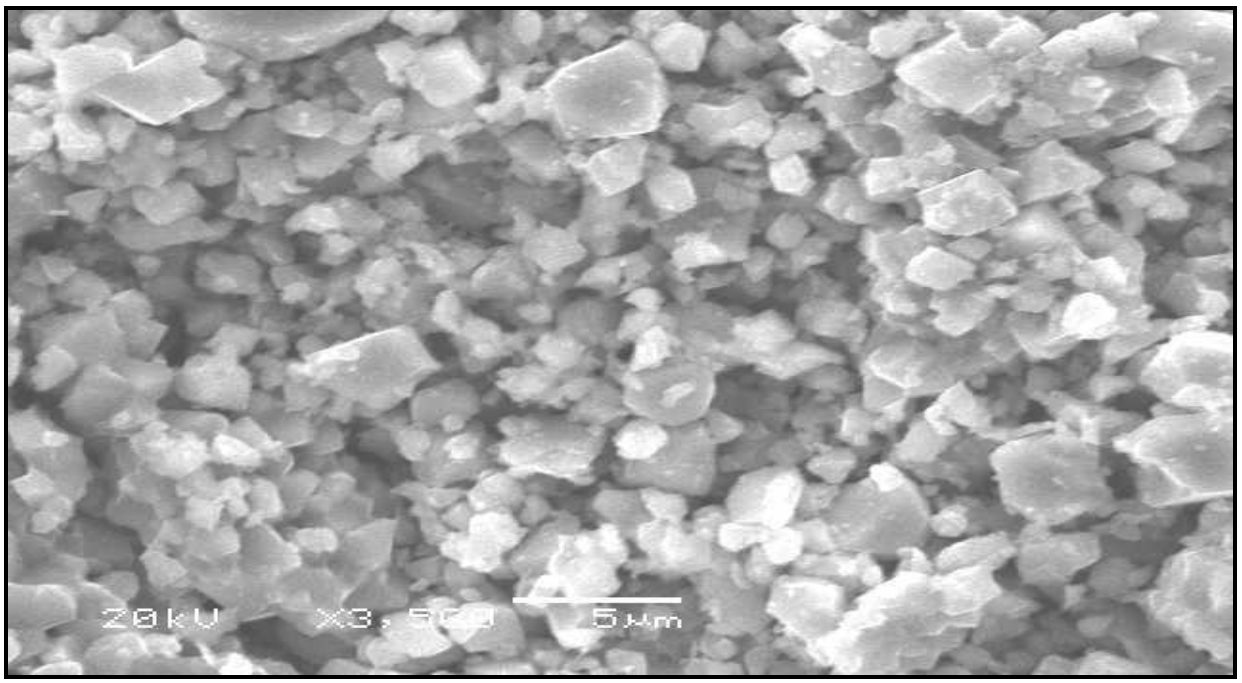

Figure 7. SEM image of $Li[V_{0.05}Cr_{0.05}Mn_{1.90}]O_4$ nanospinel.

3.5. IR spectroscopy studies

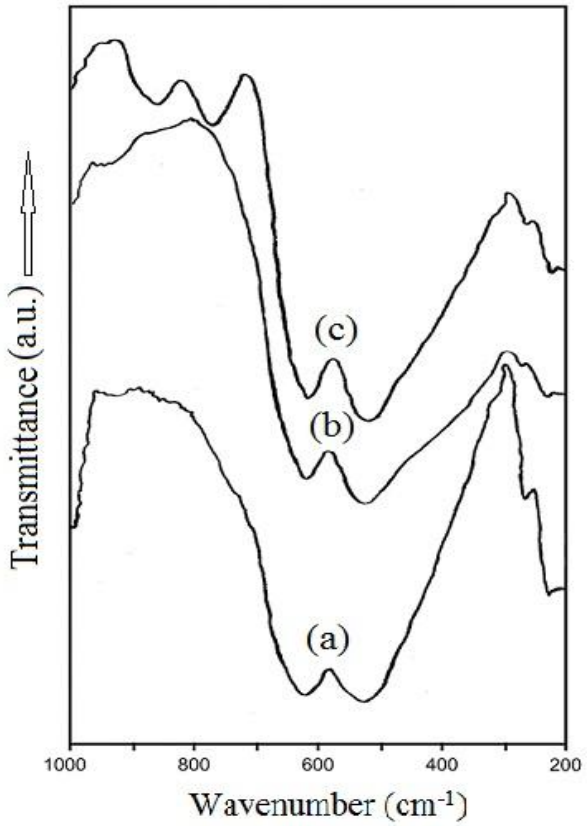

Figure 8. IR spectra of pure and co-doped Li-Mn-O spinels; (**a**) pure $LiMn_2O_4$ spinel, (**b**) co-doped $Li[V_{0.02}Cr_{0.02}Mn_{1.96}]O_4$ spinel, and (**c**) co-doped $Li[V_{0.05}Cr_{0.05}Mn_{1.90}]O_4$ spinel.

The IR spectra of pure $LiMn_2O_4$ and co-doped $Li[V_xCr_xMn_{2-2X}]O_4$ nanospinels are displayed in figure 8. IR spectra of $LiMn_2O_4$ spinel displays strong absorption bands at 221 cm^{-1}, 518 cm^{-1}, and 617 cm^{-1}, due to vibration modes of MnO_6 octahedra. The band at 260 cm^{-1} is attributable to mixed character: octahedral MnO_6 and tetrahedral LiO_4 building the cubic lattice of nano $LiMn_2O_4$. The obtained infrared spectra of the lattice vibration show broad and interfering peaks, where the structure of $LiMn_2O_4$ exhibits a charge disproportion such as $LiMn^{3+}Mn^{4+}O_4$. There are isotropic $Mn^{4+}O_6$ octahedra and locally distorted $Mn^{3+}O_6$ octahedra due to the Jahn–Teller effect. Thus, we expect to observe stretching vibration of $Mn^{4+}O_6$ and $Mn^{3+}O_6$ octahedra, which provides the broadness of the ν_{as}(Mn–O) mode.

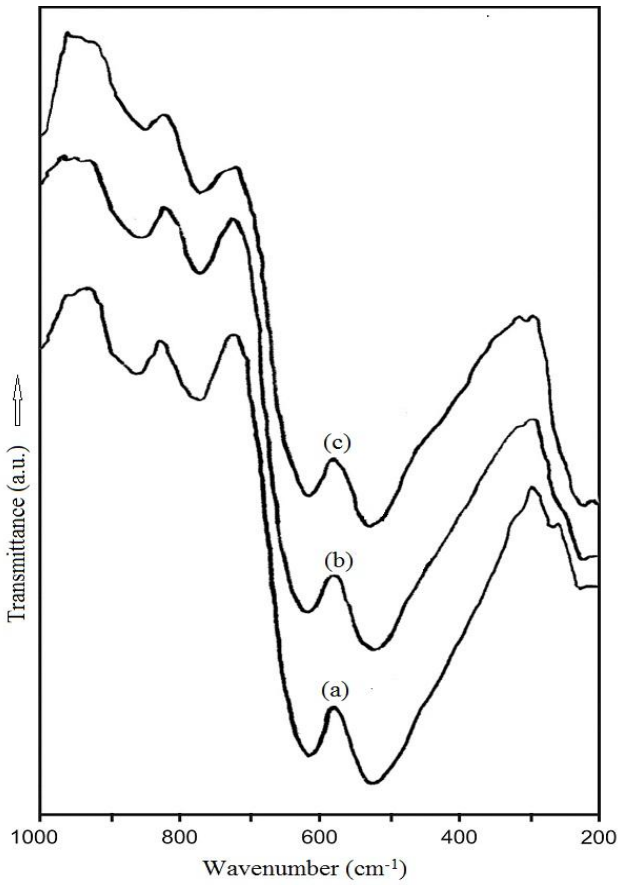

Figure 9. IR spectra of non irradiated and irradiated co-doped $Li[V_{0.05}Cr_{0.05}Mn_{1.90}]O_4$ spinel; (**a**) Non irradiated $Li[V_{0.05}Cr_{0.05}Mn_{1.90}]O_4$ spinel (**b**) $Li[V_{0.05}Cr_{0.05}Mn_{1.90}]O_4$ spinel irradiated with 10 KGy, and (**c**) $Li[V_{0.05}Cr_{0.05}Mn_{1.90}]O_4$ spinel irradiated with 30 KGy.

In the low-frequency region, the IR bands at 221 cm^{-1} and 260 cm^{-1} have mixed character due to the presence of the bending modes of O–Mn–O bands and modes of the LiO_4 group leading to interference between the peaks. This is a characteristic spectrum of $LiMn_2O_4$ spinel, in agreement with Julien et al. [34] and Wu et al. [35]. For co-doped V^{5+}, Cr^{6+} nano spinels there is red shifts from 518 to 514 and 617 to 611 cm^{-1} for x = 0.02% where the peaks shifted from 518 to 519 and from 617 to 611 cm^{-1} for x = 0.05%. This is good evidence to the insertion of V^{5+}, Cr^{6+} in octahedral position. IR

spectra of non irradiated $Li[V_{0.05}Cr_{0.05}Mn_{1.90}]O_4$ and those γ-irradiated with 10 and 30 kGy (figure 9) indicate that the samples are still nano cubic spinel but there are shifts of the main characteristic peaks from 220, 519, 611 cm^{-1} before irradiation to 224, 518, 609 cm^{-1} and 221, 520, 612 cm^{-1} for γ-irradiation with 10 and 30 kGy, respectively. In good agreement with the data obtained from x–ray diffraction studies, there are very slight changes in crystal vibration modes in case of γ-irradiated samples compared with non irradiated ones of doped samples which indicates the high stability of the spinels against γ-irradiation.

3.6. DC–electrical conductivity measurements

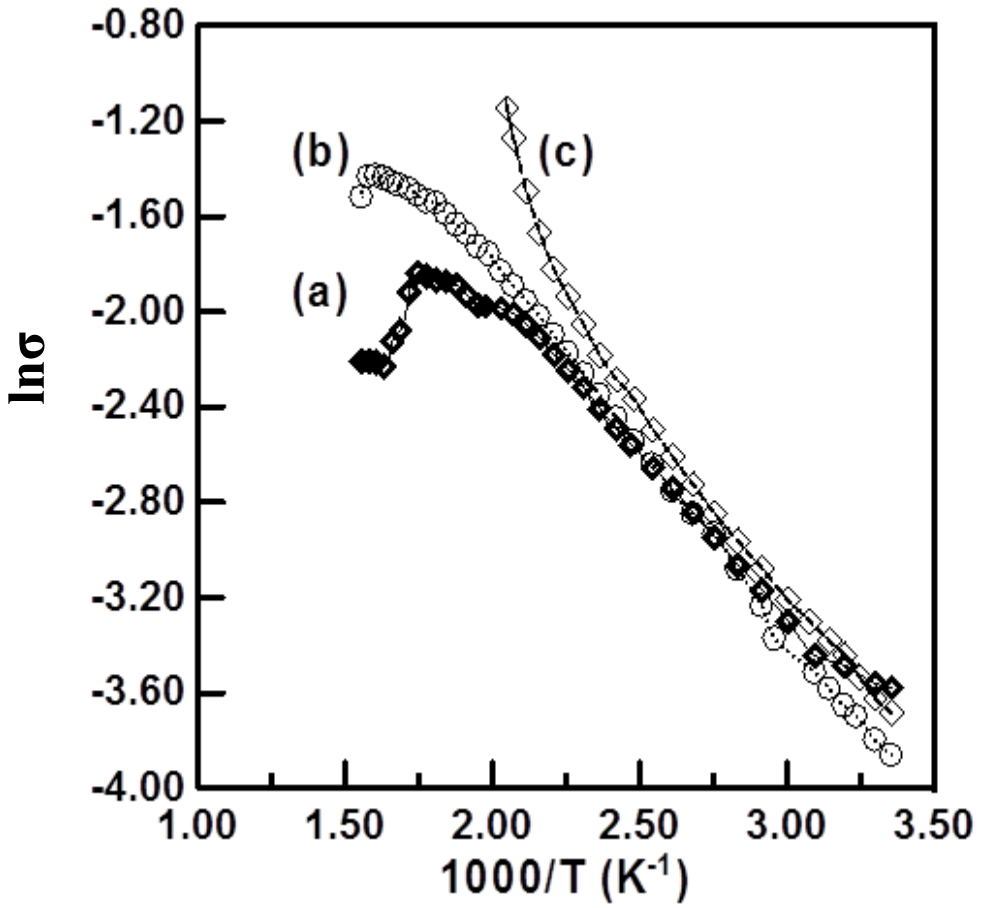

Figure 10. DC-electrical conductivity (lnσ) of pure and doped samples as a function of the reciprocal of absolute temperature (1000/T K^{-1}) for $Li[V_xCr_xMn_{2-2X}]O_4$: (**a**) $LiMn_2O_4$, (**b**) $Li[V_{0.02}Cr_{0.02}Mn_{1.96}]O_4$ and (**c**) $Li[V_{0.05}Cr_{0.05}Mn_{1.90}]O_4$.

We apply Arrhenius equation: $\sigma = \sigma^{\circ} e^{-\Delta Ea/kBT}$, where σ is the electrical conductivity at absolute temperature T, σ° is the maximum electrical conductivity (that it would have at infinite temperature), k_B is Boltzmann's constant = 8.61 X 10^{-5} eV K^{-1}, and ΔE_a is the activation energy for electrical conduction, which indicates the energy needed for an ion to jump to a free hole [36]. The measured DC electrical conductivities (lnσ) of pure and doped samples were plotted as a function of the

reciprocal of absolute temperature. The obtained plots (figure 10) proved that $LiMn_2O_4$, $Li[V_{0.02}Cr_{0.02}Mn_{1.96}]O_4$, and $Li[V_{0.05}Cr_{0.05}Mn_{1.90}]O_4$ spinels behave as extrinsic semiconductors over 25-375^oC temperature range. There are two candidates for carriers, a Li ion or a nonadiabatic small polaron of e_g electrons on Mn^{3+} ion. The DC-conductivity of $LiMn_2O_4$, $Li[V_{0.02}Cr_{0.02}Mn_{1.96}]O_4$, and $Li[V_{0.05}Cr_{0.05}Mn_{1.90}]O_4$ spinels measured up to 375^oC indicates that there are no anomalies due to due to Li-deficient. So, it can be deduced that the ionic conduction due to Li-diffusion seems difficult to play a primary role in electrical transport. Instead, a hopping-process of a nonadiabatic small polaron is likely to be the main process [37]. This confirms that the conduction in undoped and doped $LiMn_2O_4$ nanospinels occurs through small-polaron hopping between Mn^{3+} and Mn^{4+}; i.e., unpaired electrons from the e_g orbitals of high-spin Mn^{3+} (d_4) hop to neighboring low-spin Mn^{4+} (d_3) ions.

4. CONCLUSION

Pristine spinels of $LiMn_2O_4$ and $Li[V_xCr_xMn_{2-2X}]O_4$ (x = 0.02 and 0.05) have been synthesized for the first time using the solid state method to use as a cathode material in lithium rechargeable batteries. X–ray diffraction data revealed the formation of single–phase spinel with cubic crystal structure for pure and doped samples. Scanning electron micrograph images (SEM) clearly show that the grains are nano size. The stability of co-doped spinel greatly enhanced against gamma irradiation compared with pure $LiMn_2O_4$. The electrical studies confirmed the improvement of electrical properties of V^{5+} and Cr^{6+} co-doped lithium manganese oxide spinels compared with pure $LiMn_2O_4$. Therefore, V^{5+} and Cr^{6+}-modified $LiMn_2O_4$ could be employed as a very promising candidate of cathode materials for lithium-ion battery.

References

1. K. Kang, Y.S. Meng, J. Breger, C.P. Grey, G. Cedar. *Science* 311 (2006) 977.
2. J. Hassoun, K.S. Lee, Y.K. Sun, B. Scrosati. *J. Am. Chem. Soc.* 133 (2011) 3139.
3. M.J. Smith, F.M. Gray. *J. Chem. Educ.* 87 (2010) 162.
4. M. Michalska, L. Lipinska, M. Mirkowska, M. Aksienionek, R. Diduszko, M. Wasiucionek. *Solid State Ionics* 188 (2011) 160.
5. A. Iturrondobeitia, A. Goni, V. Palomares, I. Gil de Muro, L. Lezama, T. Rojo. *J. Power Sources* 216 (2012) 482.
6. D. Zhang, B.N. Popov, R.E. White, *J. Power Sources* 76 (1998) 81.
7. R.E. Liang, Z.X. Wang, H.J. Guo, X.H. Li, W.J. Peng, Z.G. Wang. *J. Power Sources* 184 (2008) 598.
8. S. Mandal, R.M. Rojas, J.M. Amarilla, P. Calle, N.V. Kosova, V.F. An- ufrienko, J.M. Rojo. *Chem Mater.* 14 (2002) 1598.
9. Y. Ein-Eli, R.C. Urian, W. Wen, S. Mukerjee. *Electrochim. Acta* 50 (2005) 1931.
10. R. Thirunakaran, A. Sivashanmugam, S. Gopukumar, C.W. Dunnill, D.H. Gregory. *J. Mater. Process Technol.* 208 (2008) 520.
11. M.M. Abou-Sekkina, A.M. Khedr, F.G. El-Metwaly. *Chem. Mater. Res.* 3 (2013) 15.
12. A.M. Khedr, M.M. Abou-Sekkina, F.G. El-Metwaly. *J. Electron. Mater.* 42 (2013) 1275.
13. A. Yamada. *J. Solid State Chem.* 122 (1996) 160.
14. D.H. Jang, Y.J. Shin, S.M. Oh. *J. Electrochem. Soc.* 143 (1996) 2204.

15. R.J. Gummow, A. de Kock, M.M. Thackeray. *Solid State Ionics* 69 (1994) 59.
16. D. Song, H. Ikuta, T. Uchida, M. Wakihara. *Solid State Ionics* 117 (1999) 151.
17. A. Iqbal, Y. Iqbal, L. Chang, S. Ahmed, T. Zhiyong, Y. Gao. *J. Nanopart. Res.* 14 (2012) 1206.
18. R.M. Rojas, J.M Amarilla, L. Pascual, J.M. Rojo, D. Kovacheva, K. Petrov. *J Power Sources* 160 (2006) 529.
19. H. Goktepe, H. Sahan, S. Patat, A. Ulgen. *Ionics* 15 (2009) 233.
20. S.G. Lu, Z.P. Cai, W.H. Jin, M.X. Li, S.T. Huang. *Rare Metals* 25 (2006) 71.
21. N.V. Kosova, E.T. Devyatkina, V.V. Kaichev, A.B. Slobodyuk, *Solid State Ionics* 192 (2011) 284.
22. F.H. El-Batal, S.M. Abo-Naf, F.M. Ezzldin. *Indian J. Pure and Appl. Phys.* 43 (2005) 579.
23. J.G. Drobny, *Ionizing Radiation and Polymers: Principles, Technology, and Applications*, 1st ed., William Andrew (2012).
24. M. Badea, A. Emandi, D. Marinescu, E. Cristurean, R. Olar, A. Braileanu, P. Budrugeac, E. Segal. *J. Therm. Anal. Cal.* 72 (2003) 525.
25. R.M. Issa, F.A. Aly, S.M. Abu-El-Wafa, F.A. El-Saied. *Thermochim. Acta* 126 (1988) 235.
26. M. Helan, L.J. Berchmans. *J. Rare Earth.* 28 (2010) 255.
27. R. Thirunakarana, K.T. Kim, Y.M. Kang, C.Y. Seo, J.Y. Lee. *J. Power Sources* 137 (2004) 100.
28. R. Thirunakarana, A. Sivashanmugama, S. Gopukumara, R. Rajalakshmib. *J. Power Sources* 187 (2009) 565.
29. 29 A. Patterson. *Phys. Rev.* 56 (1939) 978.
30. N.R. Ikhsanov. *Astrophys. Space Sci.* 184 (1991) 297.
31. F. Michael, *Radioactivity: Introduction and History*, Elsevier (2007).
32. N. Abdel-Shafi, M.M. Morsi. J. *Mater. Sci.* 32 (1986) 5185.
33. N. Li, C.J. Patrissi, G. Che, C.R. Martin. *J. Electrochem. Soc.* 147 (2000) 2044.
34. C.M. Julien, M. Mussot. *Mater. Sci. Eng. C* 97 (2003) 217.
35. C. Wu, Z. Wang, F. Wu, L. Chen, X. Hang. *Solid State Ionics* 144 (2000) 277.
36. J.O'M. Bockris, A.K.N. Reddy. "*Modern Electrochemistry*", Plenum Press (1998).
37. E.Iguchi, Y. Tokuda, H. Nakatsugawa, F. Munakata. *J. Appl. Phys.* 91, 2149 (2002).